

### Key Points:

- Hydrographic observations identify both shelf-break and coastal meltwater pathways from the western Bellingshausen Sea into the Amundsen Sea
- Differences in optical backscatter properties associated with meltwater are related to distinct coast-to-shelf break pathways
- The main pathway to the shelf break is via Seal Trough, identified as the *de facto* western boundary of the Bellingshausen Sea

### Supporting Information:

Supporting Information may be found in the online version of this article.

### Correspondence to:

M. M. Flexas,  
marf@caltech.edu

### Citation:

Flexas, M. M., Thompson, A. F., Robertson, M. L., Speer, K., Sheehan, P. M. F., & Heywood, K. J. (2024). Pathways of inter-basin exchange from the Bellingshausen Sea to the Amundsen Sea. *Journal of Geophysical Research: Oceans*, 129, e2023JC020080. <https://doi.org/10.1029/2023JC020080>

Received 23 JUN 2023

Accepted 9 MAY 2024

### Author Contributions:

**Conceptualization:** M. Mar Flexas, Andrew F. Thompson, Kevin Speer, Peter M. F. Sheehan, Karen J. Heywood

**Formal analysis:** M. Mar Flexas, Megan L. Robertson

**Funding acquisition:** Andrew F. Thompson, Kevin Speer, Karen J. Heywood

**Investigation:** M. Mar Flexas, Andrew F. Thompson, Megan L. Robertson, Kevin Speer, Peter M. F. Sheehan, Karen J. Heywood

**Methodology:** M. Mar Flexas, Andrew F. Thompson, Kevin Speer, Peter M. F. Sheehan, Karen J. Heywood

**Software:** M. Mar Flexas, Megan L. Robertson

**Validation:** M. Mar Flexas

**Visualization:** M. Mar Flexas

**Writing – original draft:** M. Mar Flexas, Andrew F. Thompson, Kevin Speer

## Pathways of Inter-Basin Exchange From the Bellingshausen Sea to the Amundsen Sea

M. Mar Flexas<sup>1</sup> , Andrew F. Thompson<sup>1</sup> , Megan L. Robertson<sup>1</sup>, Kevin Speer<sup>2</sup>, Peter M. F. Sheehan<sup>3</sup> , and Karen J. Heywood<sup>3</sup> 

<sup>1</sup>California Institute of Technology, Pasadena, CA, USA, <sup>2</sup>Florida State University, Tallahassee, FL, USA, <sup>3</sup>University of East Anglia, Centre for Ocean and Atmospheric Sciences, School of Environmental Sciences, Norfolk, UK

**Abstract** The West Antarctic Ice Sheet is experiencing rapid thinning of its floating ice shelves, largely attributed to oceanic basal melt. Numerical models suggest that the Bellingshausen Sea has a key role in setting water properties in the Amundsen Sea and further downstream. Yet, observations confirming these pathways of volume and tracer exchange between coast and shelf break and their impact on inter-sea exchange remain sparse. Here we analyze the circulation and distribution of glacial meltwater at the boundary between the Bellingshausen Sea and the Amundsen Sea using a combination of glider observations from January 2020 and hydrographic data from instrumented seals. Meltwater distributions over previously unmapped western regions of the continental shelf and slope reveal two distinct meltwater cores with different optical backscatter properties. At Belgica Trough, a subsurface meltwater peak is linked with hydrographic properties from Venable Ice Shelf. West of Belgica Trough, the vertical structure of meltwater concentration changes, with peak values occurring at greater depths and denser isopycnals. Hydrographic analysis suggests that the western (deep) meltwater core is supplied from the eastern part of Abbot Ice Shelf, and is exported to the shelf break via a previously-overlooked bathymetric trough (here named Seal Trough). Hydrographic sections constructed from seal data reveal that the Antarctic Coastal Current extends west past Belgica Trough, delivering meltwater to the Amundsen Sea. Each of these circulation elements has distinct dynamical implications for the evolution of ice shelves and water masses both locally and downstream, in the Amundsen Sea and beyond.

**Plain Language Summary** Floating ice shelves in West Antarctica are thinning, which is largely due to melting of the ice shelf base by the ocean. Here, measurements of ocean temperature, salinity, and dissolved oxygen, collected by a remotely-controlled underwater vehicle (a glider), are used to estimate the amount of ice shelf meltwater released in the Bellingshausen Sea. Distinct cores of meltwater can be distinguished by the amount of suspended material that is present in the water, which we attribute to meltwater following different circulation pathways after entering the ocean. Historical data from seals equipped with temperature and salinity sensors provide additional information about how the meltwater circulates in the region. The seal data show the presence of a narrow coastal current that brings meltwater from the Bellingshausen Sea into the Amundsen Sea. The pathways of meltwater revealed in this study suggest an important influence of the Bellingshausen Sea on ice shelves throughout West Antarctica.

## 1. Introduction

In past decades, the Antarctic Ice Sheet has experienced rapid thinning of its floating ice shelves and grounding line retreat (Konrad et al., 2018; Pritchard et al., 2012). Satellite observations starting in the 1990s reveal that both thinning and retreat have recently accelerated and are largest for the West Antarctic Ice Sheet (WAIS) (Konrad et al., 2018; Paolo et al., 2015). Changes in the thickness of WAIS ice shelves are largely attributed to oceanic basal melt (Adusumilli et al., 2020; Pritchard et al., 2012) driven by changes in the heat transport of warm Modified Circumpolar Deep Water (MCDW; Whitworth et al., 1998) intruding onto the continental shelf via bathymetric troughs. This heat transport may depend on the velocity field and/or the thickness and temperature of the MCDW layer. This process, dominant from the West Antarctic Peninsula (WAP) (Hofmann & Klinck, 1998; Klinck et al., 2004; Moffat et al., 2009) to the Amundsen Sea, is triggered by wind-driven cross-slope and cross-shelf exchange processes (Dutrieux et al., 2014; Jacobs et al., 2011; Jenkins et al., 2018; Silvano et al., 2022; Thoma et al., 2008) acting from seasonal to decadal time scales (Holland et al., 2019; Jenkins et al., 2018; Paolo et al., 2018; Schodlok et al., 2012; Wallis et al., 2023).

## Writing – review &amp; editing:

M. Mar Flexas, Andrew F. Thompson,  
Kevin Speer, Peter M. F. Sheehan, Karen  
J. Heywood

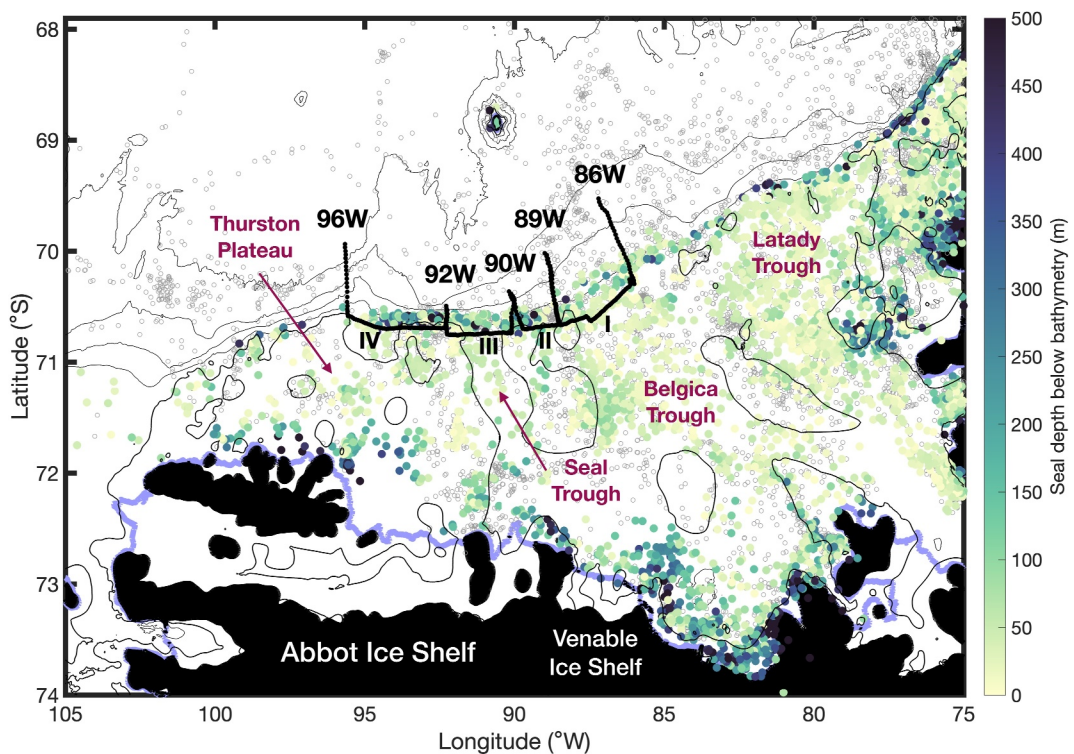


**Figure 1.** Map of the Bellingshausen Sea with major bathymetric features, floating ice shelves, and the 2020 TABASCO glider expedition (black dots/lines marking cross-slope sections 86W, 89W, 90W, 92W and 96W, and along shelf-break Sections I to IV). Seal dives from the MEOP data set are shown as gray dots, with colored dives indicating those locations where the maximum seal depth exceeds the IBCSO bathymetry. Land is shown in black, and the ice shelf edge derived from BedMachine Antarctica v2 is marked in violet. The 480 m, 1,000 m, 2,000 m and 3,000 m isobaths from the IBCSO bathymetry are shown in gray.

More recently, studies have highlighted the importance of lateral, inter-sea exchange on setting shelf water mass properties and ice shelf melt rates around Antarctica. Recent modeling studies suggest that water masses from West Antarctica can reach all regions of the Antarctic continental shelf in only 15 years (Dawson et al., 2023; Nakayama et al., 2020). Observational studies in East Antarctica show how inter-basin exchange preconditions the ocean for sea ice formation, water mass transformation, and bottom water production (Silvano et al., 2018). In particular, glacial meltwater reduces dense shelf water formation by suppressing on-shelf convection; in the absence of deep convection, warm water reaches further onto the continental shelf, increasing basal melt (Silvano et al., 2018). In West Antarctica, it has long been known that freshwater transport from the Amundsen Sea into the Ross Sea can modulate dense shelf water production (Jacobs et al., 2022; Jacobs & Giulivi, 2010). Numerical models corroborate the connection between the Amundsen-Bellingshausen seas and the Ross Sea (Assmann & Timmermann, 2005; Beckmann & Timmermann, 2001; Nakayama et al., 2014). Furthermore, modeling studies show that glacial meltwater can trigger a positive feedback mechanism that enhances ice shelf melt through changes in ocean stratification at the ice shelf front (Flexas et al., 2022). Feedbacks between the different components of the freshwater balance and their role in modifying the shelf overturning circulation and ice shelf basal melt (e.g., Bett et al., 2020; Hyogo et al., 2024; Jourdain et al., 2017; Kimura et al., 2017; Moorman et al., 2023) are critical aspects that deserve further exploration, in particular in the Bellingshausen Sea.

The Bellingshausen Sea (Figure 1) is a relatively unexplored region of West Antarctica, especially when compared with adjacent regions like the WAP or the Amundsen Sea. Recent observational efforts have highlighted some distinguishing characteristics of the Bellingshausen Sea's shelf and slope circulation. The warmest waters of the entire West Antarctic shelf seas are found in the Bellingshausen Sea (Schmidtko et al., 2014), where MCDW exhibits hydrographic properties that are only weakly modified from offshore values. Warm intrusions of MCDW enter the continental shelf at the deepest part of the Belgica Trough flowing toward the coast along the eastern side of the trough (Schulze Chretien et al., 2021). Water mass transformation peaks near the coast and

closes the shelf overturning circulation as MCDW is glacially-modified and upwells to intermediate (~200 m) levels (Ruan et al., 2021). Glacially-modified MCDW recirculates offshore, toward the continental shelf along the western side of Belgica Trough (Sheehan et al., 2023; Thompson et al., 2020). Similar circulation patterns are observed in Latady Trough, with modified warm waters eventually flowing northwards along the western side of the trough into Belgica Trough (Schulze Chretien et al., 2021).

At the shelf break, the conjunction of glacially-modified MCDW and Winter Water (WW; Mosby, 1934), the winter form of Antarctic Surface Water (AASW), leads to the formation of the Antarctic Slope Front (ASF; Jacobs, 1991), a key element of the Antarctic continental margins for deep ocean ventilation and Antarctic Bottom Water production. The ASF (and its associated current, the Antarctic Slope Current; ASC) is a quasi-circumpolar feature that originates in the Bellingshausen Sea (Thompson et al., 2020) and terminates in the southern sector of the Scotia Sea (Azaneu et al., 2017; Heywood et al., 2004) where its structure is largely determined by tides (Flexas et al., 2015). Wind stress and large-scale modes of climate variability play an important role in controlling the strength and variability of the ASC (Gill, 1973; Spence et al., 2014; Stewart & Thompson, 2012; Thompson et al., 2018). Strikingly, the only place around Antarctica where the ASF is not observed is at the WAP (Thompson et al., 2018).

Close to the coast flows the Antarctic Coastal Current (AACC), a boundary current that contributes to the renewal of shelf waters around Antarctica (Heywood et al., 1998, 2004; Jacobs, 1991). At the WAP, the AACC carries freshwater from the WAP (Moffat et al., 2008) throughout the Bellingshausen Sea (Schubert et al., 2021). The AACC varies in response to both buoyancy (Moffat et al., 2008) and wind (Holland et al., 2010; Sverdrup, 1953) forcing. Numerical simulations suggest that the AACC has a key role in setting the response to climate-induced surface forcing perturbations (e.g., freshwater fluxes from increased run-off) through its role in setting the stratification and rates of vertical heat transport in the water column (Flexas et al., 2022). A stronger AACC is associated with enhanced access of MCDW into ice shelf cavities, ultimately enhancing basal melt (Flexas et al., 2022). More generally, the AACC conveys changes in water properties occurring near the coast and enables remote responses to localized perturbations; these dynamics may occur broadly around Antarctica.

In this study we combine hydrographic data from historical instrumented seals from the Marine Mammals Exploring the Oceans Pole to Pole (MEOP) data base (Roquet et al., 2013) with data from an autonomous glider deployed in 2020 to map the circulation at the boundary between the Bellingshausen and Amundsen seas. We analyze meltwater fractions and backscatter data from the glider observations. We revisit the MEOP data base in the Bellingshausen Sea to explore bathymetry and sea surface dynamic height from seal hydrographic profiles. We detect meltwater sources from different ice shelves and find a previously overlooked trough that plays a key role collecting meltwater at the westernmost boundary of the Bellingshausen Sea. Based on these results, we discuss pathways of water property exchange (including meltwater) from the Bellingshausen Sea into the Amundsen Sea. We shed light on the AACC pathways from the Bellingshausen Sea to the Amundsen Sea and show how coastal processes in the Bellingshausen Sea are connected to the formation of the ASC/ASF. We also discuss the need to redefine the western boundary of the Bellingshausen Sea west of Belgica Trough.

The outline of the paper is as follows. Section 2 details data and methods: in Section 2.1 we describe the new glider data set; in Section 2.2 we summarize the historical MEOP seal data; in Section 2.3 we present the method used to calculate meltwater fractions. Section 3 is dedicated to present results: in Section 3.1 we present the glider observations at the shelf break, separating the data into cross-slope sections (labeled by longitude) and along-shelf-break sections (labeled using roman numerals) (Figure 1); in Section 3.2 we analyze the MEOP database seal observations over Belgica Trough and Seal Trough; in Section 3.3 we present seal observations over Thurston Plateau. In Section 4 we discuss the different pathways found toward the shelf break and along the coast. Our concluding remarks appear in Section 5.

## 2. Data and Methods

### 2.1. Glider Data

As part of the *Transport of the Antarctic Peninsula and Bellingshausen Sea: Antarctic Slope Current Origin* (TABASCO) project, Seaglider SG621 was deployed in the Bellingshausen Sea, in West Antarctica, on 1 February 2020, and surveyed the western part of the Bellingshausen Sea until 19 March 2020 (Figure 1). The region, usually heavily covered in sea ice, had particularly low sea ice concentrations in early February during this

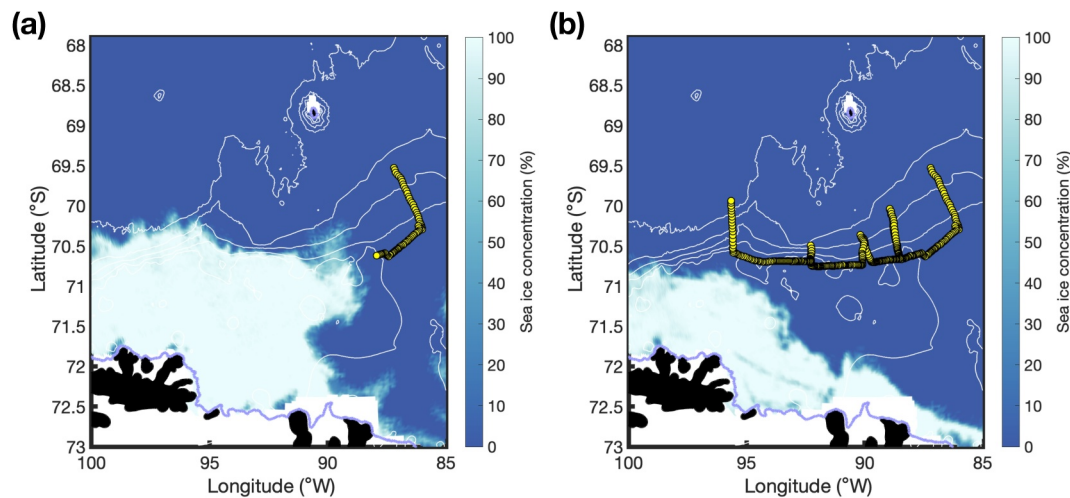


**Figure 2.** (a) Sea ice concentration on 15 February 2020 with glider positions (yellow dots) up to the date. (b) Same as panel (a), but for 17 March 2020. Land is shown in black, and the ice shelf edge is marked in violet. Bathymetry contours of 480 m, 1,000 m, 2,000 m and 3,000 m isobaths are shown in white. For names of major bathymetric features and floating ice shelves, see Figure 1.

year. From Belgica Trough to Thurston Plateau, the glider performed multiple transects crossing the continental shelf and slope. The glider transects sampled progressively westwards, following the retreat of the sea ice edge (Figure 2). This unique data set reveals the interaction of shelf and slope waters at the boundary between the Bellingshausen Sea and the Amundsen Sea at high horizontal resolution (2–4 km between profiles). To our knowledge, this is the first dedicated set of glider-based (or cruise-based) observations ever to be obtained west of Belgica Trough in the Bellingshausen Sea.

Seaglider SG621 (Ogive profile; Kongsberg Underwater Technology, Inc.) belongs to a family of underwater autonomous buoyancy-driven vehicles capable of profiling to a maximum depth of 1,000 m in a sawtooth (V-shape) pattern (Eriksen et al., 2001; Rudnick, 2016). Seaglider SG621 carried a Sea-Bird SBE3 temperature sensor and SBE4 conductivity sensor, a pressure sensor, an Aanderaa 4330F oxygen optode, WetLabs ECOpuck with two wavelengths of optical backscatter (470 and 700 nm) and chlorophyll fluorescence sensors. Following factory calibration, in situ temperature, practical salinity, and dissolved oxygen concentrations are accurate to 0.018°C, 0.01, and 2 mmol kg<sup>-1</sup>, respectively. Sensor precision is 0.0018°C and 0.0003 S m<sup>-1</sup> for temperature and conductivity, respectively, combining to a salinity precision of 0.00121. Sampling occurred approximately every 5 s, leading to a 0.5 m vertical resolution at typical vertical speeds of 0.1 m s<sup>-1</sup>.

The glider data set was processed using the University of East Anglia glider Toolbox (Queste, 2013), which includes hydrodynamic flight model corrections (Frajka-Williams et al., 2011) and thermal lag corrections (Garau et al., 2011). Depth-averaged currents (DACs) are calculated using the difference between the expected and actual surface location of the glider at the end of each profile and applying hydrodynamic flight model corrections. We use potential temperature, practical salinity and neutral density ( $\gamma^n$ ; Jackett and McDougall (1997)) unless otherwise noted. Velocity fields were constructed by calculating the geostrophic shear from the density field observed by the glider and then referencing this velocity to the DACs.

Hydrographic sections were constructed by optimally interpolating glider observations onto a regular grid with horizontal grid spacing of about 300 m. The optimally interpolated scheme uses three main parameters to smooth the data: a given number of grid points in the horizontal direction ( $d$ ), a given distance in the vertical direction ( $p$ ), and the relative error ( $\epsilon$ , for which  $0 < \epsilon < 1$ ). The parameters chosen for this study are  $d = 10$ ,  $p = 15$ , and  $\epsilon = 0.2$ , which represent horizontal length scales of 3 km and vertical length scales of 75 m (given a vertical grid spacing of 5 m).

## 2.2. Seal Data

Hydrographic data complementary to the glider observations were analyzed from the MEOP data base (Roquet et al., 2013). We use nearly 20,000 seal profiles from the Bellingshausen Sea that were originally analyzed by Zhang et al. (2016) and later by Schubert et al. (2021). This analysis extends the Schubert et al. (2021) analysis farther to the west, providing a first look at circulation patterns over Thurston Plateau and into the Amundsen Sea.

The seals are equipped with Conductivity-Temperature-Depth (CTD) Oceanography Satellite Relay Data Loggers with an in situ accuracy for pressure better than 5 db (Boehme et al., 2009). The MEOP data set is subjected to temperature and salinity calibrations, and calibrated data have estimated accuracy of better than  $\pm 0.005^{\circ}\text{C}$  for temperature and  $\pm 0.02$  for salinity (Boehme et al., 2009). The data span the years 2007–2010 and austral summer of 2013–2014 (Zhang et al., 2016). In Section 3.2 and Section 3.3 we present the seal data analysis, including water mass analysis and dynamic height anomalies, the latter calculated with a 400 m level of no motion, following Schubert et al. (2021).

The MEOP data base also provides insight into the bathymetry of the western Bellingshausen Sea, as inferred from differences between seal dive depths and the International Bathymetric Chart of the Southern Ocean (IBCSO) (Arndt et al., 2013). Because seal dives often do not reach the seafloor, we focus on those locations where the seal depth exceeds the IBCSO bathymetry. Major uncertainties in water column depth ( $>500$  m) occur close to coast and near ice shelf fronts (Figure 1). The main reason for this discrepancy is the limited ship accessibility to coastal regions, often covered by sea ice even during summer (Padman et al., 2010), and the associated lack of multibeam swath bathymetry observations. According to the seal depth data, the well-known troughs in the Bellingshausen Sea (Belgica and Latady troughs) would be  $\sim 10$ –100 m deeper than in IBCSO.

More importantly, differences between seal dive depths and the IBCSO bathymetry point to an overlooked trough west of Belgica Trough, at  $\sim 90^{\circ}\text{W}$  (hereafter named Seal Trough because of the importance of MEOP data in highlighting this feature; Figure 1), that would provide a direct path from the easternmost tip of Abbot Ice Shelf to the shelf break. Here, we provide evidence of the role of this trough in shaping the shelf circulation of the Bellingshausen Sea. Because the seal-based CTDs use ARGOS (Advanced Research and Global Observation Satellite) telemetry system, the error in position is  $\pm 5$  km (Roquet et al., 2013), comparable to the scale of the deformation radius over the continental shelf. However, the high density of the seal profiles provides statistical confidence in the updates to trough locations as well as in the circulation derived from the dynamic height analysis. This circulation should be viewed as a climatology over the period covered by the observations. While the accuracy of the seal position data is not high, it is adequate to resolve a feature as large as a trough (Seal Trough characteristic width is 35–70 km), and we have confidence in the trough location because multiple seal profiles are located within this trough. We acknowledge that seal data alone do not allow exact inference of seabed gradients, as seals do not always dive to the seafloor (though typically they forage at the sea bed). However, these data allow identification of regions where IBCSO is too shallow. The analysis presented here suggests that Seal Trough is deeper than shown by IBCSO, and we discuss its relevance in the shelf circulation of the Bellingshausen Sea.

## 2.3. Meltwater Fractions

Meltwater fractions were calculated following the Optimum Multiparameter (OMP) water mass analysis of Tomczak and Large (1989), as described by Biddle et al. (2017) for the Antarctic margins. The OMP analysis optimizes the use of a set of hydrographic variables by solving an over-determined linear set of mixing equations. The method requires representation of water masses by specific water types, finds the correct weights for the hydrographic variables (weight functions reflect the quality of each oceanographic parameter), and solves the mixing equations by minimization of the residuals.

We applied the OMP analysis to temperature, salinity and dissolved oxygen observations obtained from the glider. We chose the water types (or end members) of WW and MCDW using property-property diagrams and used canonical values for glacial meltwater (Biddle et al., 2017; Schulze Chretien et al., 2021; Sheehan et al., 2023). Water types and weight functions are detailed in (Text S1 and Figure S1 in Supporting Information S1). We explored the sensitivity of meltwater to the selection of WW and MCDW end members by running the OMP analysis for the entire range of MCDW and WW values found in the glider observations and choosing the most restrictive solution (i.e., the one with the lowest meltwater content). The meltwater fractions obtained

with other end members were as high as double the values presented here. However, the distribution of meltwater fractions was qualitatively consistent throughout the different analyses (see Supporting Information S1).

To trace the pathway of meltwater fractions from the ice shelves to the continental shelf break we took advantage of instrumented seal observations. Given that seal observations only provide temperature and salinity data, it is important to understand the role of dissolved oxygen in our estimates of meltwater fractions. For this reason, we performed an OMP analysis only using temperature and salinity data from the gliders. Meltwater fractions from glider observations without dissolved oxygen are similar in magnitude to estimates from glider observations using dissolved oxygen (Figure S2 in Supporting Information S1). They are also, importantly, located within similar density ranges. However, there are substantial differences in the horizontal locations of the maxima of meltwater fractions. For this reason, we limit our interpretation of meltwater estimates from seals to a qualitative discussion of the distribution of meltwater properties on the Bellingshausen Sea continental shelf.

### 3. Results

#### 3.1. Shelf Break Hydrographic Properties

The cross-slope glider sections span from slightly south of the continental shelf break to slightly north of the southern boundary (Bdy; Orsi et al., 1995) of the Antarctic Circumpolar Current (ACC). The Bdy is defined by the southernmost extension of Upper Circumpolar Deep Water ( $\theta > 1.5^\circ\text{C}$ ,  $S > 34.5$ ) and nearly coincides with the southernmost eastward jet associated with the ACC (Orsi et al., 1995). In our data set, the maximum potential temperature of the Bdy is  $1.85^\circ\text{C}$  at 300–400 m depth; the Southern ACC front has a temperature of  $2.0^\circ\text{C}$  at about 400 m depth (Figure 3).

In all the glider cross-slope sections, the Bdy is found over the 2,000 m isobath (Figures 1 and 3a). Moving westward from  $86^\circ\text{W}$  to  $90^\circ\text{W}$ , the Bdy (and its associated eastward jet; Figure 3b) is found progressively closer to the continental shelf as the slope steepens. The Bdy reaches its closest proximity to the shelf break at  $92^\circ\text{W}$ , and it separates offshore again at  $96^\circ\text{W}$ . The geostrophic velocity field is nearly independent of depth in the upper 1,000 m. South of the Bdy, the flow is mostly westward, with occasional flow reversals presumably related to eddies shed from the continental shelf to the open ocean. At  $92^\circ\text{W}$ , the proximity of the Bdy to the shelf break causes a reversal of the westward velocity field at depth (below  $\sim 250$  m at the shelf break; Figure 3b). The meridional tilting of isopycnals at the pycnocline ( $27.7 > \gamma^n > 27.9 \text{ kg m}^{-3}$ ) is enhanced, and isopycnals intersect the seafloor (Figure 3b), showing the typical density structure of the ASF. The Bdy sets the limit of the northward extension of WW. We use the  $-1.5^\circ\text{C}$  isotherm to estimate the thickness of the WW layer. The WW layer is thicker (150–170 m thick) south of the Bdy. At  $92^\circ\text{W}$  the Bdy is closest to the shelf break, and the thick WW layer over the shelf provides the characteristic water mass configuration of the ASF in the region (Thompson et al., 2020). Meltwater (MW) is found at the main pycnocline (Figure 3c). Noticeably, in all sections, the location of the Bdy coincides with the northward extension of large, thick MW pools. Meltwater fractions are largest ( $>0.5\%$ ) at  $90^\circ\text{W}$  and  $92^\circ\text{W}$ . The ASF/ASC system plays a main role in transporting meltwater along the slope (Heywood et al., 1998), while filaments and eddies likely shed meltwater toward the Bdy (Sheehan et al., 2023).

The glider sections taken along the shelf break span, roughly, 10 degrees of longitude (from  $86^\circ\text{W}$  to  $96^\circ\text{W}$ ). They sample through four sills, one at the western side of each along-shelf-break section (Figure 4). Sections I and II are located in Belgica Trough (Figure 1). Here, WW is relatively thick (100 m), with its core at  $\sim 100$  m. Near the bottom, the intrusion of warm, MCDW is observed in salinity ( $>34.7$ ) and dissolved oxygen ( $<140 \mu\text{mol kg}^{-3}$ ). At the pycnocline we observe two meltwater cores located close to each sill (MW fraction  $>0.5\%$ ; Figure 4d). These two meltwater cores contain relatively low backscatter ( $10^{-3.8} \text{ m}^{-1}$ ; Figure 4e) when compared with all the other waters sampled along the shelf break by the glider.

Section III is taken over a trough that connects the eastern tip of Abbot Ice Shelf to the continental shelf break (Figure 1). Section IV is taken at the shelf break off Thurston Plateau. Along these two sections, between  $91.5^\circ\text{W}$  and  $93.5^\circ\text{W}$ , the WW layer thickens (150–170 m thick; Figure 4a). At the pycnocline, we find a large meltwater core (MW fraction  $>0.5\%$ ; Figure 4d) with high backscatter properties ( $10^{-3.7} \text{ m}^{-1}$ ; Figure 4e), which are larger than those found in sections I and II (Figures 4d and 4e). To quantify the relation between meltwater and optical backscatter (Figures 5a, 5b, and 5f) we calculated the linear regression of these two variables for meltwater values higher than 0.3%. We found that a linear regression explained only 5% of the variance in Section I, but the relation

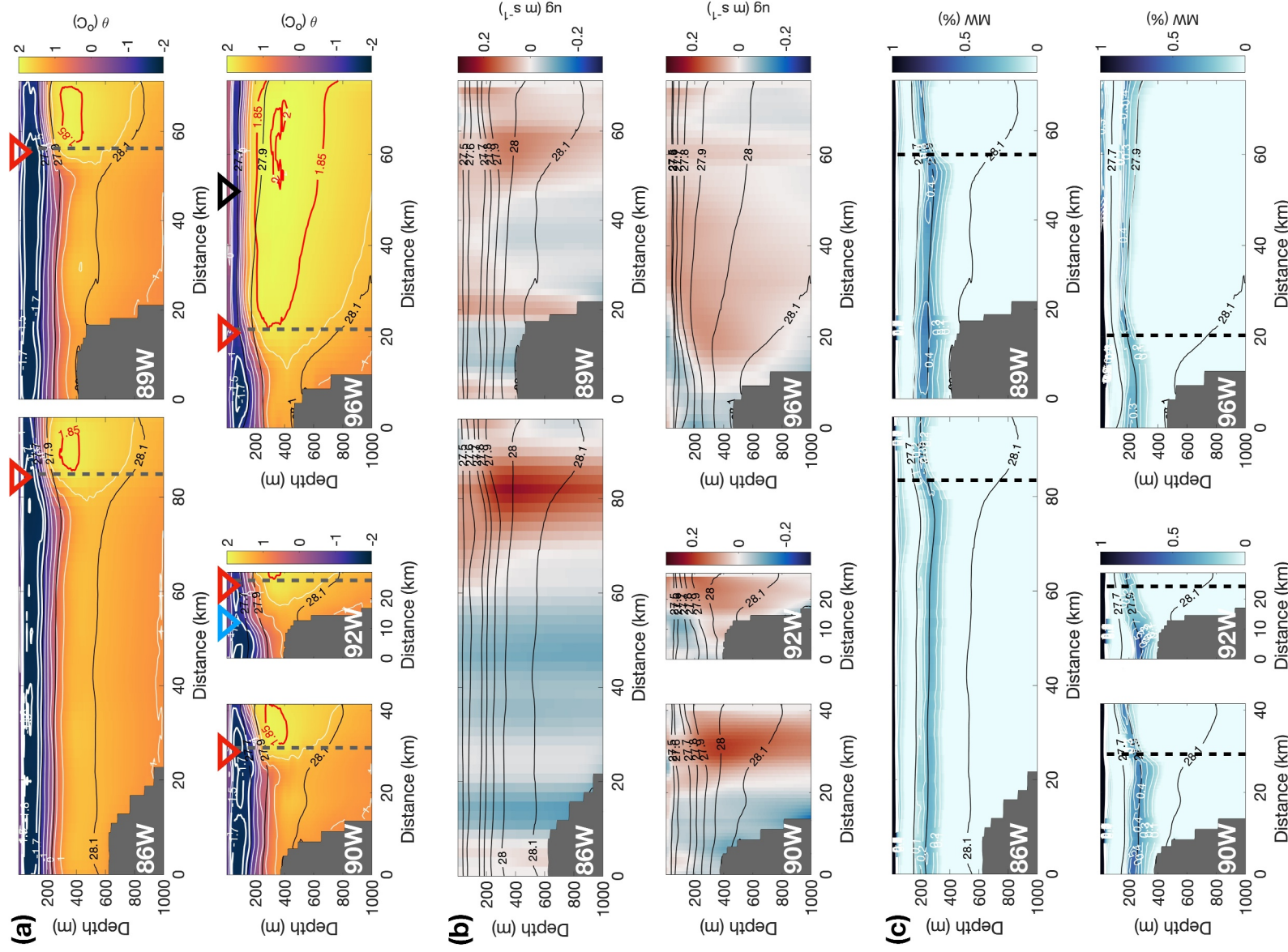


Figure 3.

increased to 30% in Section II, 36% in Section III and 48% in Section IV. A quadratic fit or cubic fit led to comparable results.

The MW core in Sections III and IV is also deeper by about 50 m (Figures 5d–5h), lies at slightly greater density levels (about  $0.02 \text{ kg m}^{-3}$ ; Figures 5c–5g) and has slightly smaller dissolved oxygen values (by about  $5 \mu\text{mol kg m}^{-3}$ ; Figures 5e–5i), compared with the MW core found in Sections I and II. These differences between MW cores were statistically tested. For instance, a two-sample *t*-test gives a mean density of  $27.87 \text{ kg m}^{-3}$  in Sections I and II and a mean density  $27.89 \text{ kg m}^{-3}$  in Sections III and IV. The difference between the two means is statistically significant ( $p = 10^{-26}$  and  $\alpha = 0.05$ , where  $p$  is the probability of the null hypothesis at the  $\alpha^*100\%$  significance level).

### 3.2. Circulation Pathways Toward the Shelf Break

Dynamic height calculated from seal observations shows a positive anomaly (of  $0.8\text{--}1.2 \text{ m}^2 \text{s}^{-2}$ ) along the coast throughout the Bellingshausen Sea (Figure 6a). The associated along-coast westward geostrophic flow, corresponding to the AACC, has a variable width of 50–150 km. These values are larger than observations of the AACC in the WAP, where the AACC is observed as a 7–20 km wide current (Moffat et al., 2008). Such differences are likely due to the nature of the seal data (sparse dives used as a climatology, rather than a snapshot hydrographic section). The AACC is correlated with fresher water near the coast (Figure 6b) and tilting isopycnals that deepen toward the coast (Figure 6c). At about  $90^\circ\text{W}$ , the AACC splits into two branches. The main part of the flow is directed toward the shelf break, following the 480-m isobath. A secondary branch continues west along the coast, toward Thurston Plateau and into the Amundsen Sea. The dynamic height also indicates a cyclonic recirculation within Belgica Trough, in agreement with Schulze Cretien et al. (2021) and Sheehan et al. (2023).

Seal-based temperature-salinity (T/S) diagrams, separated into different regions of the western Bellingshausen Sea, provide a complementary view of the circulation features observed in dynamic height. A total of eight T/S clusters of seal profile data are selected by location: three in Belgica Trough, one inside Seal Trough, one in front of Venable Ice Shelf, and three off Abbot Ice Shelf (Figure 7). We color the profiles by location (Figure 7d), and manually group the different profiles when they display similar surface-to-bottom temperature and salinity properties in temperature-salinity space. This grouping by T/S properties captures both spatial differences and seasonal variability in the water formation processes.

Water properties in front of Venable Ice Shelf (in yellow) show two different “families” with distinct T/S properties (in yellow; Figures 7a and 7b). The first family of profiles (Figure 7a) contains WW with salinity around 34.00 and temperatures below  $-1.0^\circ\text{C}$  and relatively eroded MCDW properties (34.65 in salinity and  $1.0\text{--}1.3^\circ\text{C}$ ). These profiles correspond to MEOP data from the months of March and April, with temperature values in AASW below  $-0.7^\circ\text{C}$ . Profiles east Abbot Ice Shelf (in green) and in Seal Trough (in orange) show similar T/S properties to this family (Figure 7a). We did not separate the data by years.

The second T/S family of profiles off Venable Ice Shelf (in yellow; Figure 7b) contains WW with salinity of 34.25 and MCDW properties with salinity of 34.65 and temperatures between  $1.0$  and  $1.2^\circ\text{C}$ . Profiles belonging to this T/S family correspond to MEOP data from the months of December, January and February, with temperature values in AASW between  $-1.0^\circ\text{C}$  and  $0^\circ\text{C}$ . They include seal dives off Venable Ice Shelf (in yellow) and dives over the western side of Belgica Trough (in red) (Figure 7b). We note that the temperature maxima of MCDW in front of Venable Ice Shelf (in yellow) is at the seafloor, while at Belgica Trough (in red) is at intermediate depth ( $\sim 400 \text{ m}$ ).

Last, we look at profiles collected in different parts of Belgica Trough (Figure 7c). These profiles feature WW temperatures below  $-1.2^\circ\text{C}$  (including near the freezing point) and salinity ranging between 33.50 and 34.15, and

**Figure 3.** Glider cross-slope sections along  $86^\circ\text{W}$ ,  $89^\circ\text{W}$ ,  $90^\circ\text{W}$ ,  $92^\circ\text{W}$  and  $96^\circ\text{W}$  showing (a) potential temperature,  $\theta$ , (b) geostrophic velocity referenced to depth-average currents,  $ug$ , and (c) meltwater fraction,  $MW$  (in %). In panel (a), the  $-1.5$  and  $-1.7$  isotherms are marked in white; the  $1.85^\circ\text{C}$  isotherm and the  $2.0^\circ\text{C}$  isotherm are marked in red. The location of 2,000 m isobaths is marked with a gray vertical dashed line. We use the  $-1.5^\circ\text{C}$  isotherm to estimate the thickness of the WW layer. We use the southernmost location of the  $1.85^\circ\text{C}$  isotherm to track the location of the Bdy, and the southernmost location of the  $2.0^\circ\text{C}$  isotherm to track the location of the Southern Antarctic Circumpolar Current (ACC) front. For clarity, colored triangles along the top of the panels mark the position of the Bdy (red), the Southern ACC front (black) and the Antarctic Slope Front (blue). In panel (c), a black vertical dashed line indicates uncertainty in offshore meltwater estimates because of our choice of WW and MCDW end members. In all sections, the x-axis shows distance from the glider dive closest to coast. For section locations, see Figure 1.

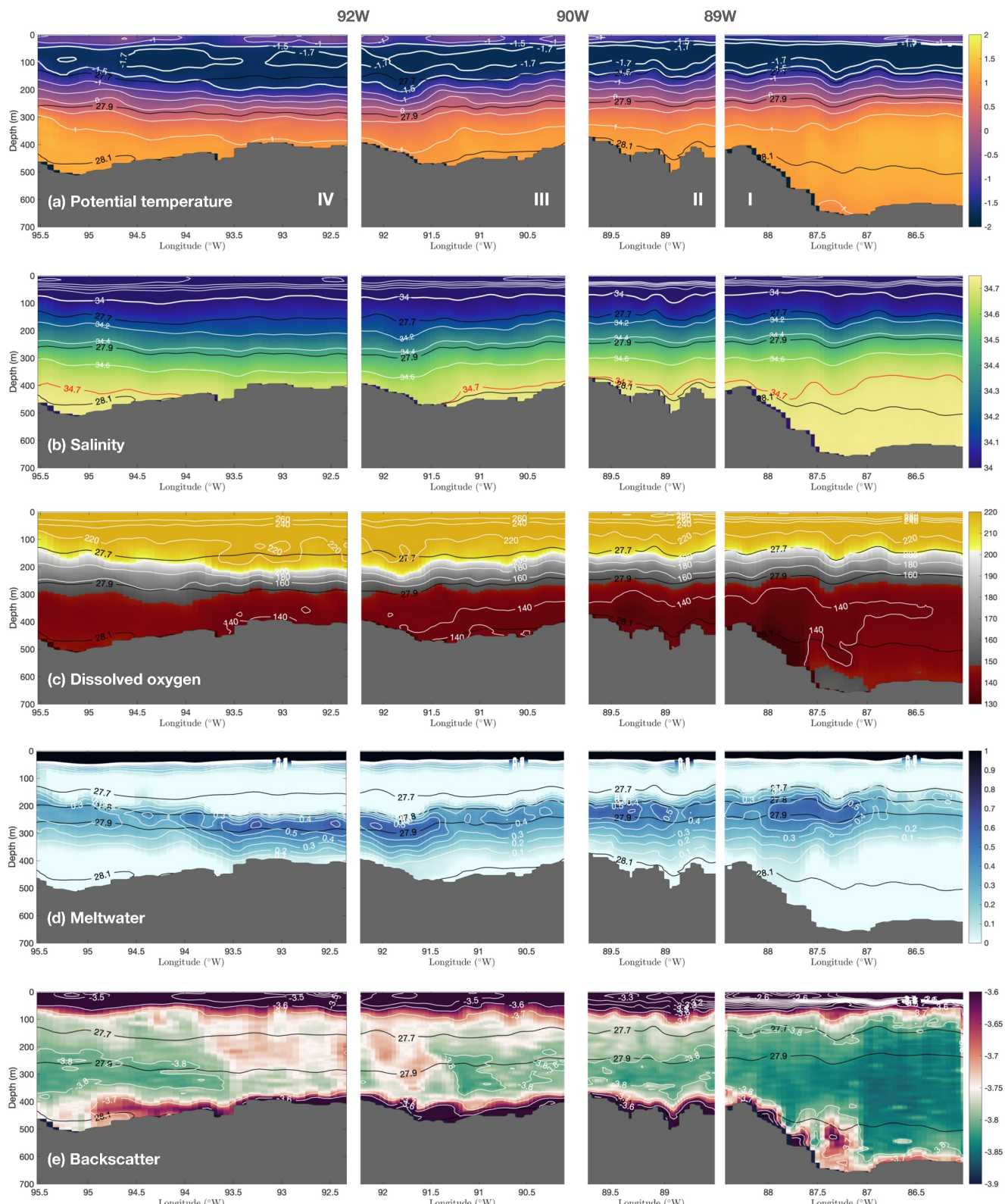


**Figure 4.** Glider sections along the shelf break (Sections I to IV) showing (a) potential temperature ( $^{\circ}\text{C}$ ), (b) salinity, (c) dissolved oxygen, DO ( $\mu\text{mol kg}^{-1}$ ), (d) meltwater fraction (%), and (e) optical backscatter ( $\text{m}^{-1}$ , in  $\log_{10}$ ). In panel (a), white bold contours of  $-1.5^{\circ}\text{C}$  and  $-1.7^{\circ}\text{C}$  are used to visualize the WW layer. In panel (b), red salinity contours of 34.7 are used to identify MCDW intrusions onto the continental shelf. In all panels, black contours of neutral density  $27.7 > \gamma^n > 27.9 \text{ kg m}^{-3}$  are used to highlight the main pycnocline. For section locations, see Figure 1.

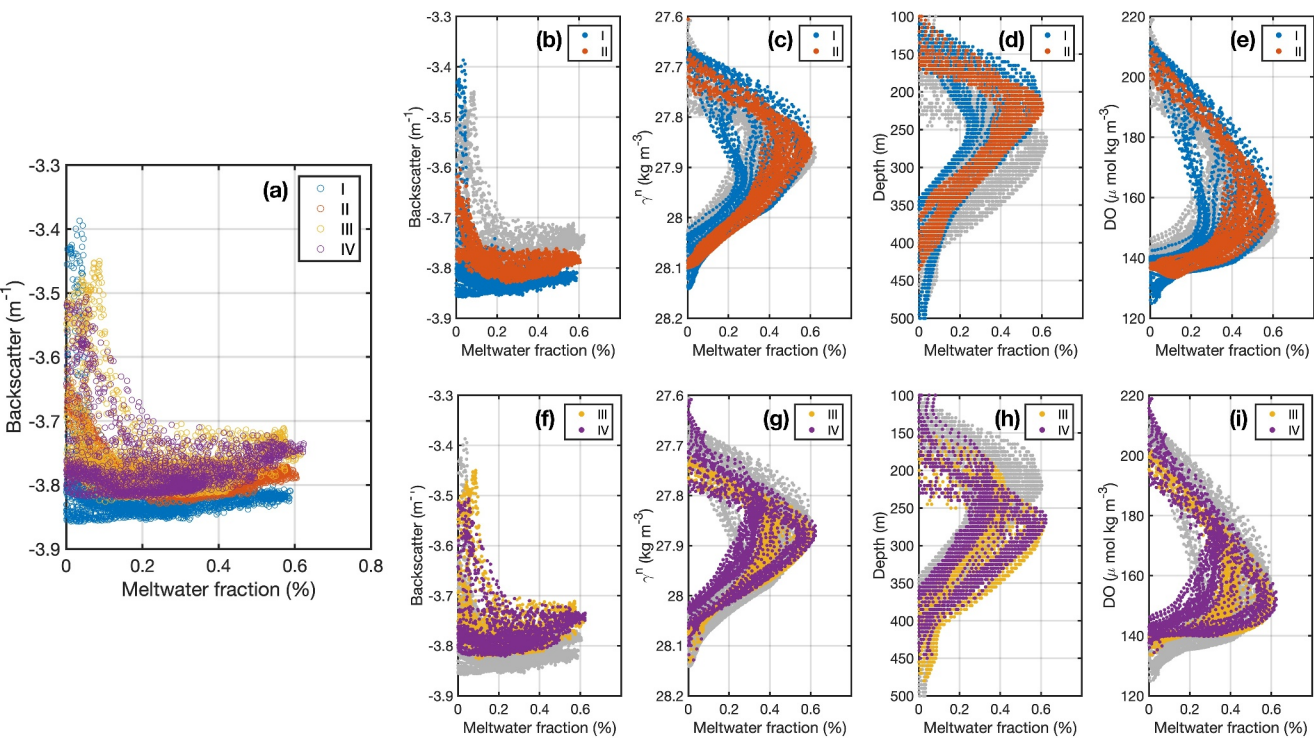


**Figure 5.** (a) Scatter plot of meltwater fraction (%) versus optical backscatter ( $\text{m}^{-1}$ , in  $\log_{10}$ ) for along shelf-break Sections I to IV (colored; see section locations in Figure 1). (b) Meltwater fraction versus optical backscatter for Sections I and II (in color; other sections are plotted in gray). (c) Meltwater fraction versus neutral density for Sections I and II. (d) Meltwater fraction versus depth (m) for Sections I and II. (e) Meltwater fraction versus dissolved oxygen ( $\mu\text{mol kg}^{-3}$ ). (f–i) Same as panels b–e, but for Sections III and IV.

warm and salty MCDW with temperature maxima at intermediate depth ( $\sim 400$  m). Temperature of AASW ranges between  $-0.5^\circ\text{C}$  and  $0.5^\circ\text{C}$ .

According to this analysis, water off Venable Ice Shelf (yellow points) flows toward the eastern Abbot Ice Shelf (green points), and from there continues northward along Seal Trough toward the shelf break (orange points; Figure 7a). A secondary route takes water from Venable Ice Shelf toward Belgica Trough (red points; Figure 7b). These results suggest a seasonal pattern in the shelf circulation of these two branches: meltwater from Venable Ice Shelf flows northward along the western side of Belgica Trough in December, January and February (Figure 7b), while in March and April, meltwater from Venable Ice Shelf flows toward Abbot Ice Shelf, and from there toward Seal Trough (Figure 7a). These results also point to a persistent recirculation inside Belgica Trough (Figure 7c), in agreement with previous works (Schulze Chretien et al., 2021; Sheehan et al., 2023). We found no similarities in T/S properties among profiles taken east of Abbot Ice Shelf (green points; Figure 7d) and west of Abbot Ice Shelf (magenta and pink points; Figure 7d).

Next, we consider the distribution of meltwater fractions in neutral density space obtained from the eight seal data clusters (Figure 8). We observe a peak of MW ( $>0.5\%$ ) centered at  $\gamma^n = 27.9 \text{ kg m}^{-3}$  off Venable Ice Shelf (panel f) and east of Abbot Ice Shelf (panel e). This peak is evident in all seal clusters, but with slight differences in density. In particular, the MW peak occurs at lighter density when it reaches Seal Trough (panel d) and the eastern and western sides of Belgica Trough (panels a and c). The seal-derived MW peaks lie at similar density classes to the MW cores observed in the glider data (Figures 3 and 4).

Additionally, there is a second MW peak inside Belgica Trough (Figure 8, panels a and b), centered at  $\gamma^n = 27.75\text{--}27.80 \text{ kg m}^{-3}$ . A peak at similar density classes is also observed at west Abbot Ice Shelf (panel g). We hypothesize that this MW peak originates from Venable Ice Shelf, where there is a large MW signature (0.5%–1.5%) at densities lighter than  $\gamma^n = 27.9 \text{ kg m}^{-3}$ . On the other hand, the MW peak is barely noticeable at the eastern side of Belgica Trough (panel c), suggesting that this peak could represent distant (remote) MW contributions from the eastern ice shelves of the Bellingshausen Sea (e.g., George VI and Stange ice shelves). Meltwater values at neutral

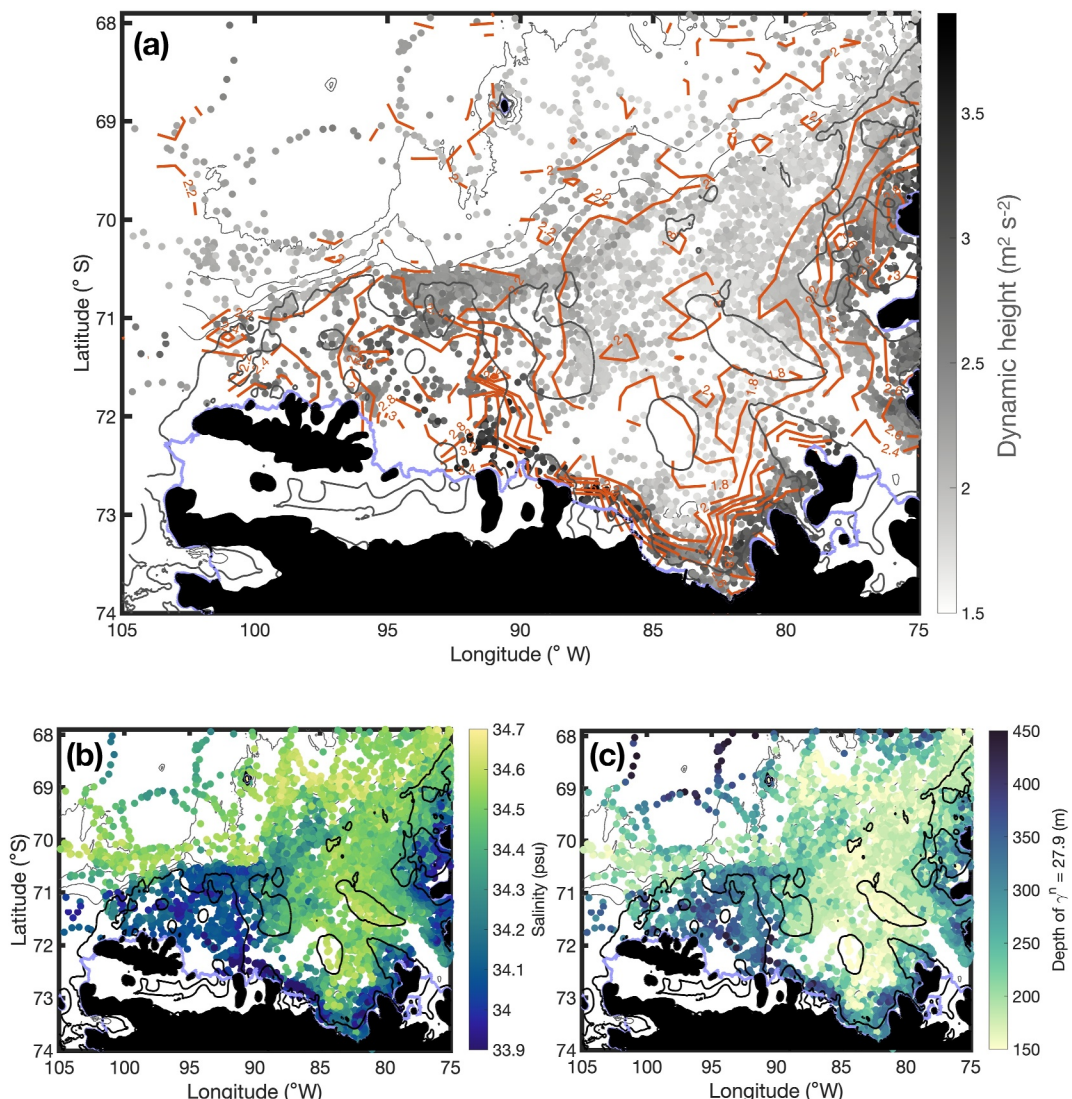


**Figure 6.** (a) Dynamic height calculated from instrumented seal data at each seal location (gray dots) and averaging (using the median value) over  $1.0^{\circ}$  longitude  $\times 0.2^{\circ}$  latitude ( $\sim 34$  km  $\times \sim 22$  km) grid cells (orange contours; isoline contour separation is  $0.2 \text{ m}^2 \text{s}^{-2}$ ). (b) Salinity at 200 m. (c) Depth of isoneutral surface  $\gamma^n = 27.9 \text{ kg m}^{-3}$ .

densities lighter than  $27.60 \text{ kg m}^{-3}$  are likely erroneous as the MW estimation method makes assumptions that are not appropriate near the surface.

### 3.3. Circulation Pathways Over Thurston Plateau

Circulation patterns over Thurston Plateau remain unclear from the analysis of T/S properties alone. Thus, to look into circulation pathways toward the Amundsen Sea, we constructed composites of hydrographic properties over three meridional sections centered at  $92^{\circ}\text{W}$ ,  $96^{\circ}\text{W}$  and  $100^{\circ}\text{W}$  (Figure 9a). The ASF appears as a density front following the shelf break (near  $70.5^{\circ}\text{S}$ ) in sections  $92^{\circ}\text{W}$  (Figure 9d) and  $96^{\circ}\text{W}$  (Figure 9c). In section  $100^{\circ}\text{W}$  (Figure 9b), the ASF is found, roughly, at  $71^{\circ}\text{S}$ . The ASF follows complex contours of the shelf break. Breaking the  $100^{\circ}\text{W}$  composite section into one-degree longitude sections evidences the continuity of the ASF. Between  $98^{\circ}\text{W}$  and  $101^{\circ}\text{W}$  the ASF is found between  $71^{\circ}\text{S}$  and  $71.2^{\circ}\text{S}$  following small-scale changes in slope direction of the shelf break (Figure S3 in Supporting Information S1).

Based on dynamic topography (Figure 6a), the AACC flows westwards, along the coast. The structure of the AACC, as observed along the  $92^{\circ}\text{W}$  composite section (Figure 9d), shows substantial freshening ( $S < 33.5$ ) of the

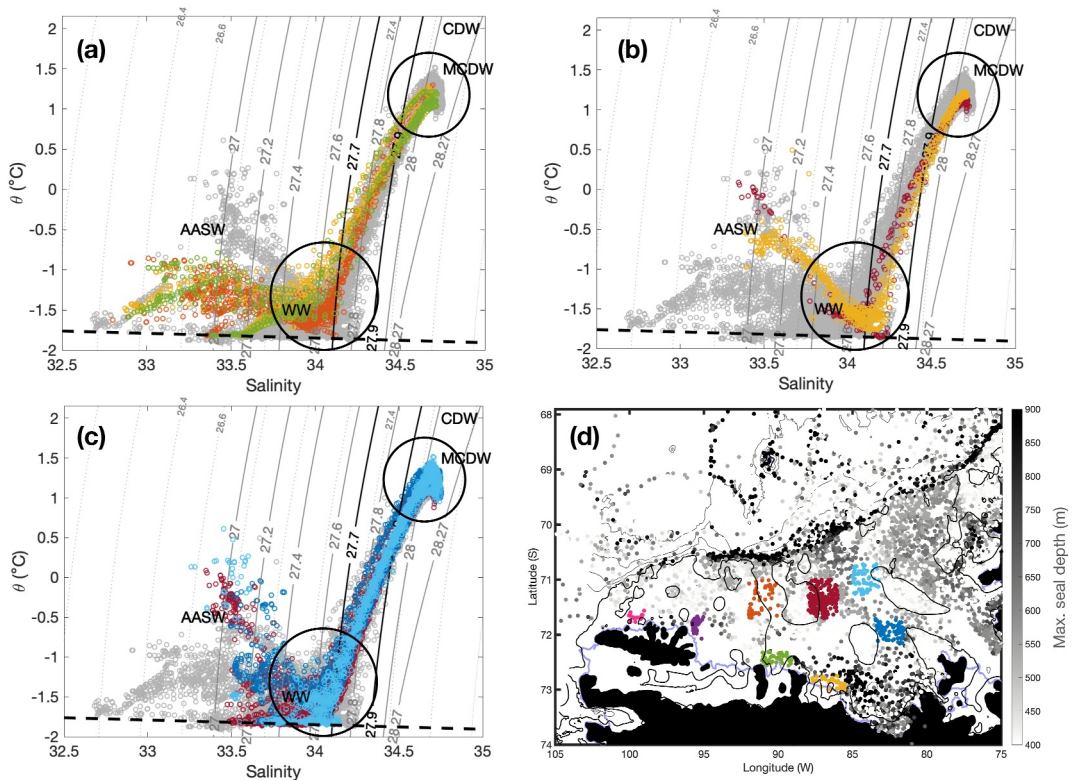


**Figure 7.** (a–c) Temperature-salinity diagrams for instrumented seal data clusters separated by geographic location (in colors; location shown in panel d). Neutral density contours are shown in gray; isoneutral values of  $27.7$  and  $27.9 \text{ kg m}^{-3}$  are highlighted in black. Main water masses are indicated by acronyms: Antarctic Surface Water (AASW), Winter Water (WW), Modified Circumpolar Deep Water (MCDW). WW and MCDW are highlighted in circles. (a) Diagrams for seal data collected in the months of March and April in front of Venable Ice Shelf (yellow), east Abbot Ice Shelf (green) and at the western side of Seal Trough (orange). Rest of clusters shown in gray. (b) Diagrams for seal data collected in the months of December, January and February in front of Venable (yellow) and at the western side of Belgica Trough (red). (c) Diagrams for all seal data collected inside Belgica Trough (at its eastern side, in light blue; at its western side, in red; and at the southern part of Belgica Trough, in dark blue). (d) Map of the Bellingshausen Sea with maximum seal depth (in gray) at each seal location. Colors show the seal clusters used in panels a–c. Two clusters at the western sector of Abbot Ice Shelf are shown in pink and magenta.

upper 200 m of the water column toward the coast. An unambiguous signature of the AACC is lost at  $96^\circ\text{W}$  (Figure 9c), although the density field is suggestive of a broader current shifted toward the central plateau. Lack of seal profiles close to the ice shelves or temporal variability on the position of the AACC are both potential explanations for the lack of an AACC signature at  $96^\circ\text{W}$ . A zoom of dynamic height over Thurston Plateau (Figure S4 in Supporting Information S1) shows the complexity of the AACC. We observe the coast-to-shelf-break pathway at  $92^\circ\text{W}$  and a clear westward flow along the coast (observed as elevated dynamic height close to the coast,  $>2.9 \text{ m}^2 \text{ s}^{-2}$ ). West of  $92^\circ\text{W}$ , the AACC continues as a westward flow along the coast. The AACC diverts toward the middle of the plateau at  $96^\circ\text{W}$  and at  $100^\circ\text{W}$ . A cluster of seal data near the coast at  $96^\circ\text{W}$  (Figure S4 in Supporting Information S1) show a wide range of dynamic height values (from  $2.2$  to  $2.6 \text{ m}^2 \text{ s}^{-2}$ ), suggesting the AACC is not steady in this position. Such variability results in a lack of AACC signature in the time-averaged dynamic height field at  $96^\circ\text{W}$  (Figure 9c). The seal data is unfortunately too intermittent in time to resolve interannual variability. Before reaching the Amundsen Sea, at the  $100^\circ\text{W}$  composite section, the AACC appears clearly again, somewhat separated from the coast ( $\sim 6$  km from the coast; at  $71.7^\circ\text{S}$ ; Figure 9b).

#### 4. Discussion

The western boundary of the Bellingshausen Sea is a poorly known region that has not been explored in much detail. The circulation of the AACC builds toward the western boundary, evidenced by decreasing salinity and increasing westward transport, where it encounters additional ice shelves and eventually the Thurston Plateau.

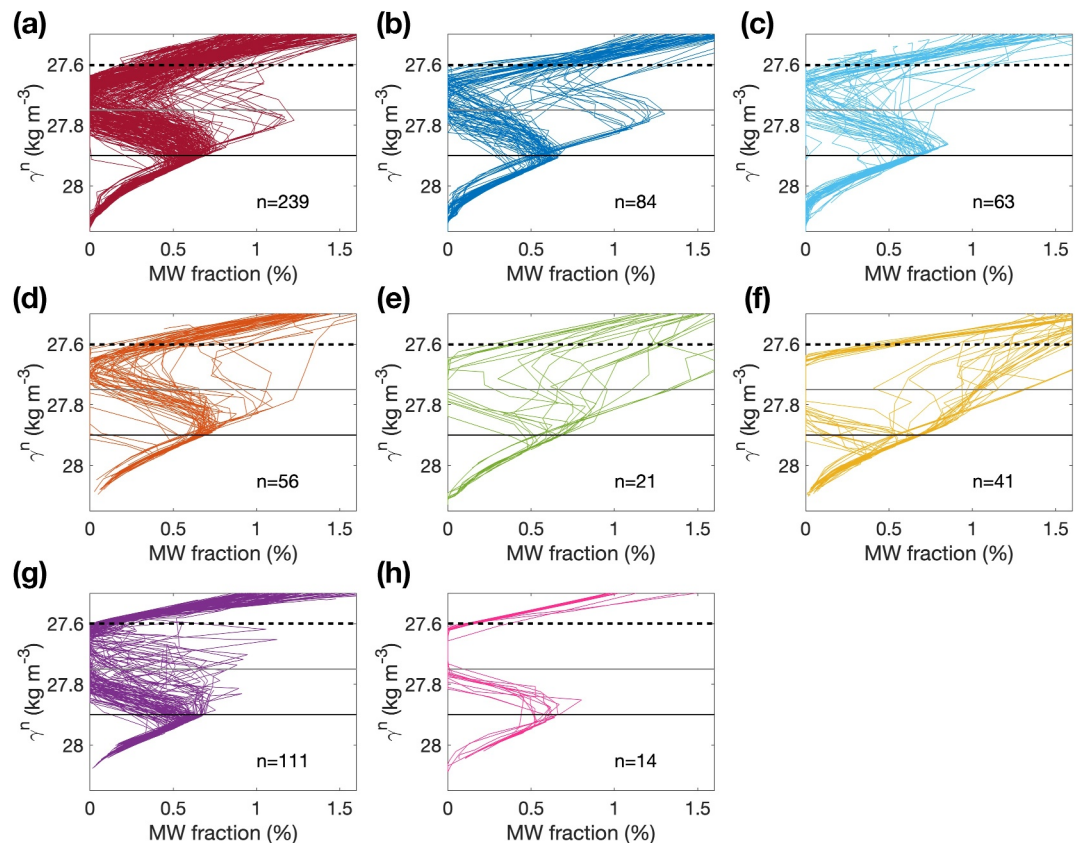


**Figure 8.** Meltwater fraction versus neutral density for seal data in panels (a–c) Belgica Trough, (d) Seal Trough, and in front of (e) Abbot east, (f) Venable, and (g–h) Abbot west Ice Shelves. Neutral density at  $\gamma^n = 27.75 \text{ kg m}^{-3}$  and  $\gamma^n = 27.90 \text{ kg m}^{-3}$  are marked with horizontal lines. A black horizontal dashed line indicates uncertainty in meltwater estimates lighter than  $\gamma^n = 27.60 \text{ kg m}^{-3}$  because the meltwater estimation method makes assumptions that are not appropriate near the surface. Location of each seal data cluster (in color) is shown in Figure 7d.

The AACC then rounds Thurston Island and flows southward to establish the route of inter-basin exchange with the Amundsen Sea.

Using glider observations and historical seal data we were able to find two main circulation pathways of meltwater export toward the Amundsen Sea: one toward the shelf break, and one near the coast. The coastal export pathway extends into the western boundary regime of the Bellingshausen Sea, largely following the westward flow of the AACC, with an apparent excursion around presently undocumented features of the bathymetry of the Thurston Plateau. The path toward the shelf break flows along both Belgica Trough (as previously documented) and Seal Trough, a previously overlooked trough west of Belgica Trough. In a few places the signature of the AACC is lost due to the variability of the current near the coast. Temporal variability in the position of the AACC and sampling gaps from a lack of seal profiles close to the ice shelves may mask the continuity of the AACC over Thurston Plateau. Nevertheless, taken together, the evidence supports a continuous AACC pathway along ice shelf fronts. Numerical models clearly show the AACC to be continuous and very close to the coast (e.g., Dawson et al., 2023). The details of the circulation linking the two seas remain to be mapped in detail, even with the extraordinary observations from the seal data set and new glider measurements, as this region is often covered with thick sea ice.

Recent models have shown a connection between the Bellingshausen and Amundsen seas, yet these models show differences in the relative importance of shelf-slope exchange versus coastal exchange (i.e., the dominance of the ASC vs. the AACC). Dawson et al. (2023), for example, find the main connection between the two seas is via the AACC. In contrast, Nakayama et al. (2014) find that the connection is mostly via the ASC/ASC. Such model differences, likely related to bathymetric constraints and other poorly constrained local sea- and glacial ice

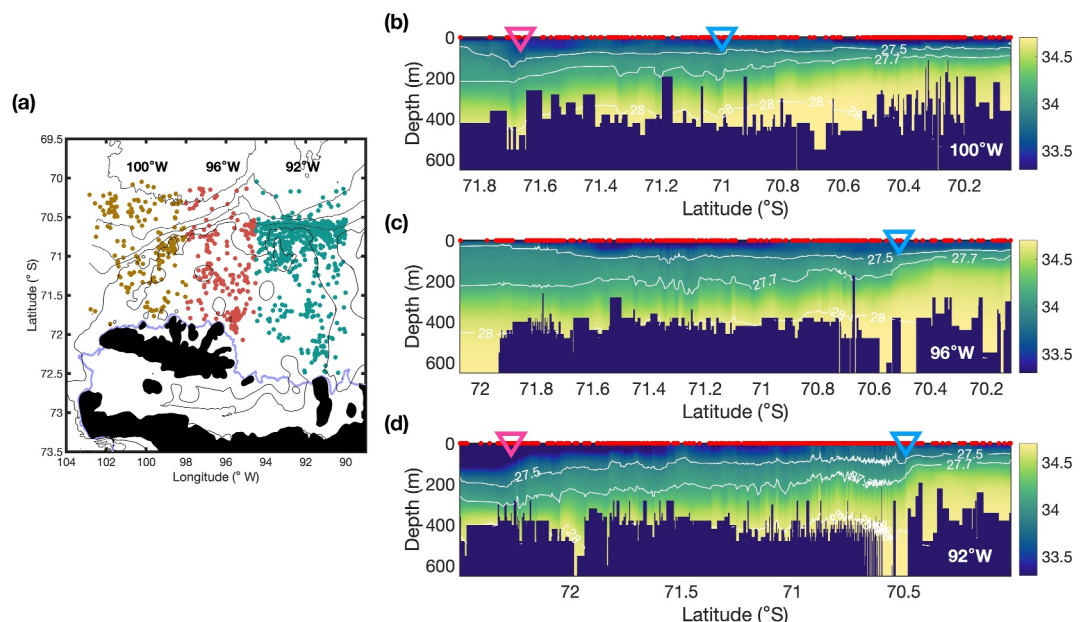


**Figure 9.** (a) Map of Thurston Plateau with seal data colored by stations used to construct composite fields along 100°W, 96°W and 92°W. (b–d) Salinity (color) and neutral density (white contours) at sections (b) 100°W, (c) 96°W, and (d) 92°W. Colored triangles along the top of the panels mark the position of the Antarctic Slope Front (blue) and the Antarctic Coastal Current (magenta). The sections are constructed using seal dive depth (Depth, m) and thus do not necessarily show the full water column depth.

conditions make it difficult to usefully assess model results. The lack of extensive multibeam bathymetry and hydrographic data along the coast makes it difficult to infer the relative importance of the coastal pathway as it continues along its path around Thurston Island. The partitioning of volume transport through these different pathways, coastal or via the shelf break, may vary across a range of timescales that could reflect decadal-scale variations in freshwater forcing from variable ice shelf melt rates, seasonal variations related to surface buoyancy forcing, or relatively short time scales as the AACC responds to wind-forced Ekman convergence near the coast.

Haigh et al. (2023) studied the effect of bathymetry on heat transport into the Amundsen Sea and found that a shallow ridge that separates the two seas enhances heat transport into the Amundsen Sea by a factor of two. Our work suggests the connection between the Bellingshausen Sea and the Amundsen Sea is more complex than indicated by the latest bathymetry, emphasizing the need for additional bathymetry observations and numerical studies to understand pathways of heat transport toward ice shelves (e.g., Haigh et al., 2023; Schodlok et al., 2012).

Glider and ship-based hydrographic data from both 2019 and 2020 show comparable amounts of meltwater on the western side of Belgica Trough (Schulze Chretien et al., 2021; Sheehan et al., 2023) and at Seal Trough in 2020 (this study). However, according to the seal-based dynamic topography, the primary boundary current, or main export pathway from the coast to the shelf break, takes place along Seal Trough. This leads us to redefine the limits of the circulation of the Bellingshausen Sea and extend the western limb of the Bellingshausen Sea's shelf circulation to include Seal Trough. The main inflow of MCDW occurs along Belgica Trough (Schulze Chretien et al., 2021) –this is expected, given that the depth of Belgica Trough at the shelf break (~800 m) is deeper than that of Seal Trough (~550 m). In contrast, the main export pathway (outflow) of glacially-modified MCDW from Venable and Abbot ice shelves takes place along Seal Trough.

According to the seal-based hydrography, the two shelf-break pathways, via Seal Trough and via Belgica Trough, show seasonal differences, with preference for export of glacially-modified MCDW along Belgica Trough from December through February, and preference for meltwater export along Seal Trough in March and April. Exploring the physical processes that give rise to seasonality in the export pathways is beyond the scope of this work and require further study in the future. Determining the pathways of exchange between the Bellingshausen

and Amundsen seas will help to validate numerical models and produce more accurate predictions of the future evolution of both seas and the ice shelves found along their coasts. Additional hydrographic data over Thurston Plateau could help to further refine the western limit of the Bellingshausen Sea, and better define the links between the shelf circulation of the Bellingshausen Sea and that of the Amundsen Sea.

Previous work emphasized the importance of the shelf circulation of the Bellingshausen Sea near the coast, on the innermost part of the upper cell of the Southern Ocean's overturning circulation (Oelerich et al., 2022; Ruan et al., 2021). In the shelf circulation of the Bellingshausen Sea, the strongest water mass transformation occurs near the coast, and it involves the erosion of MCDW properties due to mixing with less dense waters. The result of water mass transformation processes can be observed as a generalized freshening at depth (below the AACC). Then, lightened and uplifted glacially-modified MCDW near the ice shelves is carried toward the shelf break. The conjunction of MW at the pycnocline, WW at the sub-surface, and a steepening of the isopycnals at the shelf break (deeper toward the coast) leads to the formation of the ASF (Thompson et al., 2020). This occurs at the mouth of Seal Trough, near 92°W. This supports the view that, in the Bellingshausen Sea, the ASF is a buoyancy-forced mechanism, related to meltwater introduced broadly over the continental shelf, as opposed to a wind-forced one. Thompson et al. (2020) set the genesis of the ASF further to the east, at 90°W, suggesting that the location where the ASF generates varies, at least interannually. Our observations complement the studies of Thompson et al. (2020), Schulze Cretien et al. (2021), and Ruan et al. (2021) by placing the western limb of the shelf overturning circulation along the western side of Seal Trough, and the genesis of the ASF at 92°W.

Previous studies have shown that glacial meltwater discharge is associated with elevated turbidity (Meredith et al., 2018). Assuming that the primary export pathway for meltwater entering the ocean in the western Bellingshausen Sea occurs via a boundary current that follows Seal Trough, the strongest signal of accumulated fine sediment particles should be found along this trough. Furthermore, the low turbidity meltwater, which is associated with the Belgica Trough outflow, is comprised of meltwater that has a longer export pathway, possibly due to recirculation, and therefore more of the sediment could have fallen out. Larger turbidity meltwater could also indicate a path over sills or rough topography, where the water column depth is shallower, and the meltwater may incorporate sediment/particulate matter from the seafloor: the path along Seal Trough is shallower than the path along Belgica Trough, providing another potential explanation for the larger turbidity meltwater observed in Seal Trough. Nepheloid layers—deep sediment layers within the rifts—could also be an additional source of particulate matter incorporated into the meltwater signal, for example, if there is active convection that would gather up some additional sediment signal. Differing sedimentary materials deposited at the base of the ice sheet that feed the different ice shelves may potentially lead to different backscatter signals.

Recent work that combines observations and numerical modeling has attributed differences in the density and optical backscatter properties of glacial meltwater to contributions from distinct ice shelves (Sheehan et al., 2023). Our seal data analysis provides evidence of distinct meltwater pathways from Venable Ice Shelf (the shelf break pathway via Belgica Trough) and from Abbot Ice Shelf (the shelf break pathway via Seal Trough and the coastal pathway). With the present data set, it is not possible to distinguish the relative partitioning of meltwater from Venable Ice Shelf between these pathways. Both Venable and the eastern Abbot ice shelves are likely to contribute meltwater to the Seal Trough and to the coastal meltwater pathways described in this study. Additional field work would be necessary to evaluate the contribution of Venable Ice Shelf and Abbot Ice Shelves to the Bellingshausen Sea glacially-modified waters.

## 5. Conclusions

Numerical models have suggested two pathways, coastal and shelf break, for the communication of physical and biogeochemical properties between the Bellingshausen Sea and the Amundsen Sea. Yet, the sparse historical data from the western Bellingshausen Sea has limited the ability to constrain these pathways with observations. In this study, measurements from both a glider and instrumented seals enable the assessment of meltwater distributions and meltwater export pathways in this region based on an optimum multiparameter analysis. The observations provide evidence that both pathways between these shelf seas exist.

The shelf break pathway is mapped in detail across multiple cross-shelf/slope hydrographic sections. Previously identified meltwater outflow along the western side of Belgica Trough represents an accumulation of melt from Venable Ice Shelf. Yet, farther west, the vertical structure and concentration of meltwater at the shelf break undergo an abrupt change, with peak values occurring at deeper depths and denser density layers. Independent

glider-mounted sensors indicate that these two meltwater cores feature different properties in optical backscatter, which suggests two distinct pathways. The high turbidity meltwater, likely supplied from the easternmost tip of Abbot Ice Shelf, is exported to the shelf break via a previously-overlooked bathymetric trough west of Belgica Trough. Dynamic height and temperature-salinity diagram analysis from the seal data also support these conclusions.

In this study, the fate of the AACC is traced into the western Bellingshausen Sea for the first time. Multiple composite hydrographic sections constructed from the seal data reveal that the AACC, a surface-intensified, buoyant boundary current, extends west past Belgica Trough, carrying part of the meltwater from the Bellingshausen Sea to the Amundsen Sea. Meltwater pathways from the shelf break, and the AACC, eventually meet in a complex circulation over Thurston Plateau.

The relative importance of these two pathways is difficult to resolve from these observations alone because of the different temporal scales they resolve: the glider data show snapshots from 2020 while the seal data represent a climatology over multiple years. Resolving spatial and temporal variability in these transport pathways is key since this influences shelf residence time scales as well as the modification of physical and biogeochemical properties over the continental shelf. Adequate modeling of these dynamics is also critical to predicting the evolution of the Amundsen and Bellingshausen seas and their vulnerable fringing ice shelves in coming decades.

## Data Availability Statement

The seaglider SG621 data used in this study is available at NOAA's National Centers for Environmental Information (NCEI), <https://data.nodc.noaa.gov/cgi-bin/iso?id=gov.noaa.nodc:0210639>. The glider data set was processed using the University of East Anglia (UEA) glider Toolbox (Queste, 2013), available at <https://bitbucket.org/bastienqueste/uea-seaglider-toolbox/downloads/>. Historical instrumented seal data from the MEOP data base (Roquet et al., 2013) were downloaded from <https://www.meop.net/database/meop-databases/meop-ctd-database.html>. The data analysis and figures produced for this manuscript were performed using Matlab R2017b (MATLAB, 2017), available at noindent <https://www.mathworks.com/products/matlab.html>. The bathymetry used in this study is a blend from IBCSO v1.0 (Arndt et al., 2013), currently at [https://ibcso.org/previous\\_releases/](https://ibcso.org/previous_releases/), and BedMachine Antarctica v2 (Morlighem et al., 2020), available at <https://sites.ps.uci.edu/morlighem/dataproducts/bedmachine-antarctica/>.

## Acknowledgments

This work was funded by National Science Foundation Grants OPP-1644172 (M.M. F., A.F.T. and M.L.R.), OPP-1643679 (K. S.), and OCE-1658479 (K.S.); National Aeronautics and Space Administration Grant 80NSSC21K0916 (M.M.F. and A.F. T.); and the Internal Research and Technology Development program (Earth 2050 project), Jet Propulsion Laboratory, California Institute of Technology (M.M. F. and A.F.T.). This research has received funding to the COMPASS project from the European Research Council under the European Union's Horizon 2020 research and innovation programme (Grant agreement n° 741120). We thank glider pilots from the University of East Anglia and from the California Institute of Technology for their help piloting SG621 (a.k.a. Moby) during the TABASCO cruise. Special thanks to Gillian Damerell for her help with the glider processing toolbox and to Michael Schodlok for providing the IBCSO-BedMachine blended bathymetry file. We thank our colleagues Ryan Schubert, Lena Schulze Cretien and Ruth Moorman for helpful conversations. We thank two anonymous reviewers for their time and valuable comments that helped improve this manuscript.

## References

Adusumilli, S., Fricker, H. A., Medley, B., Padman, L., & Siegried, M. R. (2020). Interannual variations in meltwater input to the Southern Ocean from Antarctic ice shelves. *Nature Geoscience*, 13(9), 616–620. <https://doi.org/10.1038/s41561-020-0616-z>

Arndt, J. E., Schenke, H. W., Jakobsson, M., Nitsche, F. O., Buys, G., Goleby, B., et al. (2013). The International Bathymetric Chart of the Southern Ocean (IBCSO) version 1.0 – A new bathymetric compilation covering circum-Antarctic waters [Dataset]. *Geophysical Research Letters*, 40(12), 3111–3117. <https://doi.org/10.1002/grl.50413>

Assmann, K. M., & Timmermann, R. (2005). Variability of dense water formation in the Ross Sea. *Ocean Dynamics*, 55(2), 68–87. <https://doi.org/10.1007/s10236-004-0106-7>

Azaneu, M., Heywood, K. J., Queste, B., & Thompson, A. F. (2017). Variability of the Antarctic slope current system in the Northwestern Weddell sea. *Journal of Physical Oceanography*, 47(12), 2977–2997. <https://doi.org/10.1175/JPO-D-17-0030.1>

Beckmann, A., & Timmermann, R. (2001). Circumpolar influences on the Weddell sea: Indication of an Antarctic circumpolar coastal wave. *Journal of Climate*, 14(17), 3785–3792. [https://doi.org/10.1175/1520-0442\(2001\)014\(3785:CIOTWS\)2.0.CO;2](https://doi.org/10.1175/1520-0442(2001)014(3785:CIOTWS)2.0.CO;2)

Bett, D. T., Holland, P. R., Garabato, A. C. N., Jenkins, A., Dutrieux, P., Kimura, S., & Fleming, A. (2020). The impact of the Amundsen Sea freshwater balance on ocean melting of the West Antarctic ice sheet. *Journal of Geophysical Research: Oceans*, 125(9), 6854–6870. <https://doi.org/10.1029/2020JC016305>

Biddle, L. C., Heywood, K. J., Kaiser, J., & Jenkins, A. (2017). Glacial meltwater identification in the Amundsen Sea. *Journal of Physical Oceanography*, 47(4), 933–954. <https://doi.org/10.1175/jpo-d-16-0221>

Boehme, L., Lovell, P., Biuw, M., Roquet, F., Nicholson, J., Thorpe, S. E., et al. (2009). Technical note: Animal-borne CTD-satellite relay data loggers for real-time oceanographic data collection. *Ocean Science*, 5(4), 685–695. <https://doi.org/10.5194/os-5-685-2009>

Dawson, H. R. S., Morrison, A. K., England, M. H., & Tamisitt, V. (2023). Pathways and timescales of connectivity around the Antarctic continental shelf. *Journal of Geophysical Research: Oceans*, 128(2), e2022JC018962. <https://doi.org/10.1029/2022JC018962>

Dutrieux, P., De Rydt, J., Jenkins, A., Holland, P. R., Ha, H. K., Lee, S. H., et al. (2014). Strong sensitivity of Pine Island ice-shelf melting to climatic variability. *Science*, 343(6167), 174–178. <https://doi.org/10.1126/science.1244341>

Eriksen, C. C., Osse, T. J., Light, R. D., Wen, T., Lehman, T. W., Sabin, P. L., et al. (2001). Seaglider: A long-range autonomous underwater vehicle for oceanographic research. *IEEE Journal of Oceanic Engineering*, 26(4), 424–436. <https://doi.org/10.1109/48.972073>

Flexas, M. M., Schodlok, M. P., Padman, L., Menemenlis, D., & Orsi, A. H. (2015). Role of tides on the formation of the Antarctic slope front at the Weddell-Scotia Confluence. *Journal of Geophysical Research: Oceans*, 120(5), 3658–3680. <https://doi.org/10.1002/2014jc010372>

Flexas, M. M., Thompson, A. F., Schodlok, M. P., Zhang, H., & Speer, K. (2022). Antarctic Peninsula warming triggers enhanced basal melt rates throughout West Antarctica. *Science Advances*, 8(32), 1–11. <https://doi.org/10.1126/sciadv.abj9134>

Frajka-Williams, E., Eriksen, C. K., Rhines, P. B., & Harcourt, R. R. (2011). Determining vertical water velocities from Seaglider. *Journal of Atmospheric and Oceanic Technology*, 28(12), 1641–1656. <https://doi.org/10.1175/2011jtecho830.1>

Garau, B., Ruiz, S., Zhang, W. G., Pascual, A., Heslop, E., Kerfoot, J., & Tintore, J. (2011). Thermal lag correction on slocum CTD glider data. *Journal of Atmospheric and Oceanic Technology*, 28(9), 1065–1071. <https://doi.org/10.1175/jtech-d-10-05030.1>

Gill, A. E. (1973). Circulation and bottom water production in the Weddell Sea. *Deep-Sea Research*, 20(2), 111–140. [https://doi.org/10.1016/0011-7471\(73\)90048-x](https://doi.org/10.1016/0011-7471(73)90048-x)

Haigh, M., Holland, P. R., & Jenkins, A. (2023). The influence of bathymetry over heat transport onto the Amundsen Sea continental shelf. *Journal of Geophysical Research: Oceans*, 128(5), e2022JC019460. <https://doi.org/10.1029/2022JC019460>

Heywood, K. J., Locarnini, R. A., Frew, R. D., Denis, P. F., & King, B. A. (1998). Transport and water masses of the Antarctic Slope Front system in the eastern Weddell Sea. In S. S. Jacobs & R. F. Weiss (Eds.), *Ocean, ice, and atmosphere: Interactions at the Antarctic continental margin*. *Antarct. Res. Ser.* (Vol. 75, pp. 203–214). AGU. <https://doi.org/10.1029/ar075p0203>

Heywood, K. J., Naveira Garabato, A. C., Stevens, D. P., & Muench, R. D. (2004). On the fate of the Antarctic slope front and the origin of the Weddell front. *Journal of Geophysical Research*, 109(C6), C06021. <https://doi.org/10.1029/2003jc002053>

Hofmann, E. E., & Klinck, J. M. (1998). Thermohaline variability of the waters overlying the west Antarctic Peninsula continental shelf. In S. S. Jacobs & R. F. Weiss (Eds.), *Ocean, ice, and atmosphere: Interactions at the Antarctic continental margin*. *Antarct. Res. Ser.* (Vol. 75, pp. 67–81). AGU. <https://doi.org/10.1029/ar075p0067>

Holland, P. R., Bracegirdle, T. J., Dutrieux, P., Jenkins, A., & Steig, E. J. (2019). West Antarctic ice loss influenced by internal climate variability and anthropogenic forcing. *Nature Geoscience*, 12(9), 718–724. <https://doi.org/10.1038/s41561-019-0420-9>

Holland, P. R., Jenkins, A., & Holland, D. M. (2010). Ice and ocean processes in the Bellingshausen Sea, Antarctica. *Journal of Geophysical Research*, 115(C5), C05020. <https://doi.org/10.1029/2008JC005219>

Hyogo, S., Nakayama, Y., & Mensah, V. (2024). Modeling ocean circulation and ice shelf melt in the Bellingshausen Sea. *Journal of Geophysical Research: Oceans*, 129(3), e2022JC019275. <https://doi.org/10.1029/2022JC019275>

Jackett, D. R., & McDougall, T. J. (1997). A neutral density variable for the world's oceans. *Journal of Physical Oceanography*, 27(2), 237–263. [https://doi.org/10.1175/1520-0485\(1997\)027<0237:andvft>2.0.co;2](https://doi.org/10.1175/1520-0485(1997)027<0237:andvft>2.0.co;2)

Jacobs, S. S. (1991). On the nature and significance of the Antarctic slope front. *Marine Chemistry*, 35(1–4), 9–24. [https://doi.org/10.1016/s0304-4203\(09\)90005-6](https://doi.org/10.1016/s0304-4203(09)90005-6)

Jacobs, S. S., & Giulivi, C. F. (2010). Large multidecadal salinity trends near the Pacific–Antarctic continental margin. *Journal of Climate*, 23(17), 4508–4525. <https://doi.org/10.1175/2010JCLI3284.1>

Jacobs, S. S., Giulivi, C. F., & Dutrieux, P. (2022). Persistent Ross Sea freshening from imbalance West Antarctic ice shelf melting. *Journal of Geophysical Research: Oceans*, 127(3), e2021JC017808. <https://doi.org/10.1029/2021JC017808>

Jacobs, S. S., Jenkins, A., Giulivi, C. F., & Dutrieux, P. (2011). Stronger ocean circulation and increased melting under Pine Island Glacier ice shelf. *Nature Geoscience*, 4(8), 519–523. <https://doi.org/10.1038/ngeo1188>

Jenkins, A., Shoosmith, D., Dutrieux, P., Jacobs, S., Kim, T. W., Lee, S. H., et al. (2018). West Antarctic ice sheet retreat in the Amundsen Sea driven by decadal oceanic variability. *Nature Geoscience*, 11(10), 733–738. <https://doi.org/10.1038/s41561-018-0207-4>

Jourdain, N. C., Mathiot, P., Merino, N., Durand, G., Sommer, J. L., Spence, P., et al. (2017). Ocean circulation and sea-ice thinning induced by melting ice shelves in the Amundsen Sea. *Journal of Geophysical Research: Oceans*, 122(3), 2550–2573. <https://doi.org/10.1002/2016JC012509>

Kimura, S., A. Jenkins, A., Regan, H., Holland, P. R., Assmann, K. M., Whitt, D. B., et al. (2017). Oceanographic controls on the variability of ice-shelf basal melting and circulation of glacial meltwater in the Amundsen Sea Embayment, Antarctica. *Journal of Geophysical Research: Oceans*, 122(12), 10131–10155. <https://doi.org/10.1002/2017JC012926>

Klinck, J. M., Hofmann, E. E., Beardsley, R. C., Salihoglu, B., & Howard, S. (2004). Water-mass properties and circulation on the west Antarctic Peninsula continental shelf in austral fall and winter 2001. *Deep-Sea Res. II*, 51(17–19), 1925–1946. <https://doi.org/10.1016/j.dsr2.2004.08.001>

Konrad, H., Shepherd, A., Gilbert, L., Hogg, A. E., McMillan, M., Muir, A., & Slater, T. (2018). Net retreat of Antarctic glacier grounding lines. *Nature Geoscience*, 11(4), 258–262. <https://doi.org/10.1038/s41561-018-0082-z>

MATLAB. (2017). MATLAB version: 9.3.0 (R2017b). Natick, Massachusetts, United States [Software]. *The MathWorks Inc.* Retrieved from <https://www.mathworks.com>

Meredith, M. P., Falk, U., Bers, A. V., Mackensen, A., Schloss, I. R., Barlett, E. R., et al. (2018). Anatomy of a glacial meltwater discharge event in an Antarctic cove. *Philosophical Transactions of the Royal Society A*, 376(2122), 1–17. <https://doi.org/10.1098/rsta.2017.0163>

Moffat, C., Beardsley, R. C., Owens, B., & van Lipzig, N. (2008). A first description of the Antarctic Peninsula coastal current. *Deep-Sea Research II*, 55(3–4), 277–293. <https://doi.org/10.1016/j.dsr2.2007.10.003>

Moffat, C., Owens, B., & Beardsley, R. C. (2009). On the characteristics of Circumpolar Deep Water intrusions to the west Antarctic Peninsula continental shelf. *Journal of Geophysical Research*, 114(C5), C05017. <https://doi.org/10.1029/2008JC004955>

Moorman, R., Thompson, A. F., & Wilson, E. A. (2023). Thermal responses to Antarctic ice shelf melt in an eddy-rich global ocean-sea ice model. *Geophysical Research Letters*, 50(16), e2023GL104724. <https://doi.org/10.1029/2023GL104724>

Morlighem, M., Rignot, E., Binder, T., Blankenship, D. D., Drews, R., Eagles, G., et al. (2020). Deep glacial troughs and stabilizing ridges unveiled beneath the margins of the Antarctic ice sheet [Dataset]. *Nature Geoscience*, 13(2), 132–137. <https://doi.org/10.1038/s41561-019-0510-8>

Mosby, H. (1934). The waters of the Atlantic Antarctic ocean. *Det Norske Viden. Akad., Science Research, Norwegian Antarctic Exped.*, 1(11), 1927–1928.

Nakayama, Y., Timmermann, R., & Hellmer, H. H. (2020). Impact of West Antarctic ice shelf melting on Southern Ocean hydrography. *The Cryosphere*, 14(7), 2205–2216. <https://doi.org/10.5194/tc-14-2205-2020>

Nakayama, Y., Timmermann, R., Rodehacke, C. B., Schroeder, M., & Hellmer, H. H. (2014). Modeling the spreading of glacial meltwater from the Amundsen and Bellingshausen seas. *Geophysical Research Letters*, 41(22), 7942–7949. <https://doi.org/10.1002/2014gl061600>

Oerlich, R., Heywood, K. J., Damerell, G. M., & Thompson, A. F. (2022). Wind-induced variability of warm water on the southern Bellingshausen Sea continental shelf. *Journal of Geophysical Research: Oceans*, 127(11), e2022JC018636. <https://doi.org/10.1029/2022JC018636>

Orsi, A. H., Whitworth, T., & Nowlin, W. D. (1995). On the meridional extent and fronts of the Antarctic Circumpolar Current. *Deep-Sea Research I*, 42(5), 641–673. [https://doi.org/10.1016/0967-0637\(95\)00021-w](https://doi.org/10.1016/0967-0637(95)00021-w)

Padman, L., Costa, D. P., Bolmer, T., Goebel, M. E., Huckstadt, L. A., Jenkins, A., et al. (2010). Seals map bathymetry of the Antarctic continental shelf. *Geophysical Research Letters*, 37(21), L21601. <https://doi.org/10.1029/2010GL044921>

Paolo, F. S., Fricker, H. A., & Padman, L. (2015). Volume loss from Antarctic ice shelves is accelerating. *Science*, 348(6232), 327–331. <https://doi.org/10.1126/science.aaa0940>

Paolo, F. S., Padman, L., Fricker, H. A., Adusumilli, S., Howard, S., & Siegried, M. R. (2018). Response of Pacific-sector Antarctic ice shelves to the El Niño/Southern Oscillation. *Nature Geoscience*, 11(2), 121–126. <https://doi.org/10.1038/s41561-017-0033-0>

Pritchard, H. D., Ligtenberg, S. R. M., Fricker, H. A., Vaughan, D., Van den Broeke, M. R., & Padman, L. (2012). Antarctic ice-sheet loss driven by basal melting of ice shelves. *Nature*, 484(7395), 502–505. <https://doi.org/10.1038/nature10968>

Queste, B. (2013). Hydrographic observations of oxygen and related physical variables in the North Sea and western Ross Sea Polynya (Ph.D. thesis). [Software] (p. 251). University of East Anglia. <https://ueaprints.uea.ac.uk/id/eprint/48678>

Roquet, F., Wunsch, C., Forget, G., Heimbach, P., Guinet, C., Reverdin, G., et al. (2013). Estimates of the Southern Ocean general circulation improved by animal-borne instruments [Dataset]. *Geophysical Research Letters*, 40(23), 6176–6180. <https://doi.org/10.1002/2013gl058304>

Ruan, X., Speer, K., Thompson, A. F., Schulze Chretien, L. M., & Shoosmith, D. R. (2021). Ice-shelf meltwater overturning in the Bellingshausen Sea. *Journal of Geophysical Research: Oceans*, 126(5), e2020JC016957. <https://doi.org/10.1029/2020JC016957>

Rudnick, D. L. (2016). Ocean research enabled by underwater gliders. *Annual Review of Marine Science*, 8(1), 519–541. <https://doi.org/10.1146/annurev-marine-122414-033913>

Schmidtko, S., Heywood, K. J., Thompson, A. F., & Aoki, S. (2014). Multidecadal warming of Antarctic waters. *Science*, 346(6214), 1227–1231. <https://doi.org/10.1126/science.1256117>

Schodlok, M. P., Menemenlis, D., Rignot, E., & Studinger, M. (2012). Sensitivity of the ice-shelf/ocean system to the sub-ice-shelf cavity shape measured by NASA IceBridge in Pine Island Glacier, West Antarctica. *Annals of Glaciology*, 53(60), 156–162. <https://doi.org/10.3189/2012aog60a073>

Schubert, R., Thompson, A. F., Bebieva, Y., & Speer, K. (2021). The Antarctic coastal current in the Bellingshausen Sea. *The Cryosphere*. <https://doi.org/10.5194/tc-2021-43>

Schulze Chretien, L. M., Thompson, A. F., Flexas, M. M., Speer, K., Swaim, N., Oelerich, R., et al. (2021). The shelf circulation of the Bellingshausen Sea. *Journal of Geophysical Research: Oceans*, 126(5), e2020JC016871. <https://doi.org/10.1029/2020JC016871>

Sheehan, P. M. F., Heywood, K. J., Thompson, A. F., Flexas, M. M., & Schodlok, M. P. (2023). Sources and pathways of glacial meltwater in the Bellingshausen Sea, Antarctica. *Geophysical Research Letters*, 50(14). <https://doi.org/10.1029/2023gl102785>

Silvano, A., Holland, P. R., Naughten, K. A., Dragomir, O., Dutrieux, P., Adrian Jenkins, Y. S., et al. (2022). Baroclinic ocean response to climate forcing regulates decadal variability of ice-shelf melting in the Amundsen Sea. *Geophysical Research Letters*, 49(24), e2022GL100646. <https://doi.org/10.1029/2022GL100646>

Silvano, A., Rintoul, S. R., Peña-Molino, B., Hobbs, W. R., van Wijk, E., Aoki, S., et al. (2018). Freshening by glacial meltwater enhances melting of ice shelves and reduces formation of Antarctic Bottom Water. *Science Advances*, 4. <https://doi.org/10.1126/sciadv.aap9467>

Spence, P., Griffies, S. M., England, M. H., Hogg, A. M. C., Saenko, O. A., & Jourdain, N. C. (2014). Rapid subsurface warming and circulation changes of Antarctic coastal waters by poleward shifting winds. *Geophysical Research Letters*, 41(13), 4601–4610. <https://doi.org/10.1002/2014GL060613>

Stewart, A. L., & Thompson, A. F. (2012). Eddy-mediated transport of warm circumpolar deep water across the Antarctic shelf break. *Geophysical Research Letters*, 42(2), 432–440. <https://doi.org/10.1029/2014GL062281>

Sverdrup, H. U. (1953). The currents off the coast of Queen Maud Land. *Norsk geogr. Tidsskr.*, 14(1), 239–249. <https://doi.org/10.1080/00291955308551737>

Thoma, M., Jenkins, A., Holland, D., & Jacobs, S. (2008). Modelling circumpolar deep water intrusions on the Amundsen Sea continental shelf, Antarctica. *Geophysical Research Letters*, 35(18), L18602. <https://doi.org/10.1029/2008gl034939>

Thompson, A. F., Speer, K. G., & Schulze Chretien, L. M. (2020). Genesis of the Antarctic slope current in West Antarctica. *Geophysical Research Letters*, 47(16). <https://doi.org/10.1029/2020GL087802>

Thompson, A. F., Stewart, A. L., Spence, P., & Heywood, K. J. (2018). The Antarctic slope current in a changing climate. *Reviews of Geophysics*, 56(4), 741–770. <https://doi.org/10.1029/2018rg000624>

Tomczak, M., & Large, D. G. B. (1989). Optimum multiparameter analysis of mixing in the thermocline of the eastern Indian Ocean. *Journal of Geophysical Research*, 94(C11), 16141–16149. <https://doi.org/10.1029/JC094C11p16141>

Wallis, B. J., Hogg, A. E., van Wessem, J. M., Davison, B. J., & van den Broeke, M. R. (2023). Widespread seasonal speed-up of west Antarctic Peninsula glaciers from 2014 to 2021. *Nature Geoscience*, 16(3), 231–237. <https://doi.org/10.1038/s41561-023-01131-4>

Whitworth, T., Orsi, A. H., Kim, S. J., Nowlin, W. D. Jr., & Locarnini, R. A. (1998). Water masses and mixing near the Antarctic slope front. In S. S. Jacobs & R. F. Weiss (Eds.), *Ice, and atmosphere: Interactions at the antarctic continental margin* (Vol. 75, pp. 1–27). Antarctic Research Series. Amer. Geophys. Union. <https://doi.org/10.1029/ar075p0001>

Zhang, X., Thompson, A. F., Flexas, M. M., Roquet, F., & Bornemann, H. (2016). Circulation and meltwater distribution in the Bellingshausen Sea: From shelf break to coast. *Geophysical Research Letters*, 43(12), 6402–6409. <https://doi.org/10.1029/2016GL068998>

## References From the Supporting Information

BeaIRD, N., Straneo, F., & Jenkins, W. J. (2015). Spreading of Greenland meltwaters in the ocean revealed by noble gases. *Geophysical Research Letters*, 42(18), 7705–7713. <https://doi.org/10.1020/2015gl065003>

Biddle, L. C., Loose, B., & Heywood, K. J. (2019). Upper ocean distribution of glacial meltwater in the Amundsen Sea, Antarctica. *Journal of Geophysical Research: Oceans*, 124(10), 6854–6870. <https://doi.org/10.1029/2019JC015133>

Tomczak, M. (1981). A multi-parameter extension of temperature/salinity diagram techniques for the analysis of non-isopycnal mixing. *Progress in Oceanography*, 10(3), 147–171. [https://doi.org/10.1016/0079-6611\(81\)90010-0](https://doi.org/10.1016/0079-6611(81)90010-0)